Direct and indirect light emissions from layered $ReS_{2-x}Se_x$ ($0 \le x \le 2$)

2017 Nanotechnology 28 235203

(http://iopscience.iop.org/0957-4484/28/23/235203)

IOP Publishing Nanotechnology
Nanotechnology 28 (2017) 235203 (9pp) https://doi.org/10.1088/1361-6528/aa6f51

Direct and indirect light emissions from layered $ReS_{2-x}Se_x$ ($0 \leqslant x \leqslant 2$)

Ching-Hwa Ho[1,2], Zhan-Zhi Liu[1] and Min-Han Lin[1]

[1] Graduate Institute of Applied Science and Technology, National Taiwan University of Science and Technology, Taipei 106, Taiwan
[2] Graduate Institute of Electro-Optical Engineering and Department of Electronic and Computer Engineering, National Taiwan University of Science and Technology, Taipei 106, Taiwan

E-mail: chho@mail.ntust.edu.tw

Received 24 March 2017, revised 12 April 2017
Accepted for publication 25 April 2017
Published 18 May 2017

Abstract

ReS_2 and $ReSe_2$ have recently been enthusiastically studied owing to the specific in-plane electrical, optical and structural anisotropy caused by their distorted one-layer trigonal (1 T) phase, whereas other traditional transition-metal dichalcogenides (TMDCs, e.g. MoS_2 and WSe_2) have a hexagonal structure. Because of this special property, more and versatile nano-electronics and nano-optoelectronics devices can be developed. In this work, 2D materials in the series $ReS_{2-x}Se_x$ ($0 \leqslant x \leqslant 2$) have been successfully grown by the method of chemical vapor transport. The direct and indirect resonant emissions of the complete series of layers can be simultaneously detected by polarized micro-photoluminescence (μPL) spectroscopy when the thickness of the $ReS_{2-x}Se_x$ is greater than ~70 nm. When it is less than 70 nm, only three direct excitonic emissions—E_1^{ex}, E_2^{ex} and E_S^{ex}—are detected. For the thick (bulk) $ReS_{2-x}Se_x$, more stacking of the ReX_2 monolayers even flattens and shifts the valence-band maximum from Γ to the other K- or M-related points, thus leading to the coexistence of direct and indirect resonant light emissions from the *c*-plane ReX_2. The transmittance absorption edge of each bulk ReX_2 (a few microns thick) usually has a lower energy than those of the direct E_1^{ex} and E_2^{ex} excitonic emissions to form indirect absorption. The coexistence of direct and indirect emissions in ReX_2 is a unique characteristic of a 2D layered semiconductor possessing triclinic low symmetry.

Supplementary material for this article is available online

Keywords: rhenium dichalcogenides, in-plane anisotropy, dichroic emissions, excitons

(Some figures may appear in colour only in the online journal)

Introduction

ReX_2 (X = S, Se) compounds are transition-metal dichalcogenides (TMDCs) [1] crystallized in the distorted $CdCl_2$-type layer structure with triclinic symmetry (space group $P\bar{1}$) [2–4]. Unlike other layered TMDCs (e.g. MoS_2 group) [5] that possess a two-layer hexagonal (2 H) or three-layer rhombohedral (3 R) phase, ReX_2 compounds have a distorted one-layer trigonal (1 T) structure formed by many of the Re_4 'diamond shape' units interconnected (clustered) into long chains that lie parallel to the layer plane's *b* axis (see supplementary information SI—figure S1 is available at stacks.iop.org/NANO/28/235203/mmedia) [6]. The 1T-TMX_2 phases with d electron counts from d^1 to d^3 (e.g. VII Re) may easily form various patterns of structural distortion caused by metal–metal bond interaction [7]. Over the past 20 years we have discovered many examples of in-plane optical [8–11], electrical [12, 13] and structural anisotropy [14] in the triclinic 2D layers owing to the distortion caused by Re_4 cluster chains in ReX_2, and which has recently resulted in enthusiastic study of various potential applications of the 2D material, such as in a polarization-sensitive photodetector [15, 16], an axial-dependent digital inverter [17], a flexible optoelectronics device [18], field-effect transistors [19] and an electrochemical capacitor for energy storage [20, 21]. A ReS_2 polymer-gate electrical double layer transistor (EDLT) even

reveals that monolayer ReS_2 ($t \sim 0.75$ nm) and multilayer ReS_2 ($t \sim 10$ nm) have totally different conduction behaviors of conductivity suppression and metal–insulation transition owing to the ionic disorder caused by the ionic polymer gate [22]. Thin-multilayer ReS_2 has been claimed to be a direct semiconductor with a photoluminescence (PL) peak at ~1.5 eV, while the PL energy of monolayer ReS_2 is around 1.6 eV due to the effect of 2D quantum confinement [23]. Although previous absorption results in bulk ReS_2 and $ReSe_2$ showed an indirect band edge [24, 25], the occurrence of PL emission in a thick ReX_2 layer still poses a challenge in determining whether the band-edge nature of ReX_2 is direct or indirect. The weaker decoupling between monolayers and the triclinic low symmetry of ReS_2 may be key factors in preserving the direct band gap from thin monolayers into thick bulk crystal.

In this study, we demonstrate polarization-dependent micro-photoluminescence (μPL) measurements of triclinic multilayers of $ReS_{2-x}Se_x$ with different selenium compositions of $x = 0$, 0.2, 0.4, 0.6, 0.8, 1.0, 1.2, 1.4, 1.6, 1.8 and 2.0 at 300 K. Layered crystals of the entire series $ReS_{2-x}Se_x$ ($0 \leqslant x \leqslant 2$) were grown by the method of chemical vapor transport using I_2 as the transport agent (for experimental details see SI). For the first time, the excitonic emissions of band-edge E_1^{ex} and E_2^{ex} in $ReS_{2-x}Se_x$ series multilayers with a clear polarization dependence have been detected in the polarized μPL spectra. The E_1^{ex} and E_2^{ex} excitons in the light emission spectra of the $ReS_{2-x}Se_x$ multilayers (MLs) are similar to those detected in bulk crystals using modulation spectroscopy [8, 14]. As the Se composition is increased, the energy difference (ΔE) between E_2^{ex} and E_1^{ex} of the $ReS_{2-x}Se_x$ series decreases owing to the change in lattice constant and ion potential in the $ReS_{2-x}Se_x$ series when Se substitutes for S. An indirect related emission below E_1^{ex} and E_2^{ex} can be detected especially for a layer thickness (t) greater than 70 nm. For $t > 1$ μm, some emission peaks with energies lower than the band-edge exciton can be detected in the μPL spectra. They may come from the indirect resonant emissions of the rhenium dichalcogenides with emission energies close to the indirect absorption edge of the bulk $ReS_{2-x}Se_x$ [3]. The weaker coupling between the ion potentials of each monolayer may lead to the coexistence of direct and indirect light emissions that appear in bulk $ReS_{2-x}Se_x$ of distorted 1 T phase. The band-edge emissions give the layered $ReS_{2-x}Se_x$ the potential for application in flexible light-emitting devices in the near infrared (NIR) region.

Results and discussion

Figure 1(a) shows the unpolarized μPL spectra of MLs in the $ReS_{2-x}Se_x$ ($0 \leqslant x \leqslant 2$) series near the band edge. The specimen samples of MLs are exfoliated from bulk crystals of $ReS_{2-x}Se_x$ using Scotch tape, and then transferred to a SiO_2/Si substrate. Figure 1(b) shows the atomic force microscopy (AFM) images and measurement thickness for three selected specimens of $ReS_{0.8}Se_{1.2}$, $ReS_{1.8}Se_{0.2}$ and $ReS_{1.6}Se_{0.4}$. Owing to the in-plane mechanical anisotropy of the ReX_2 crystal (see

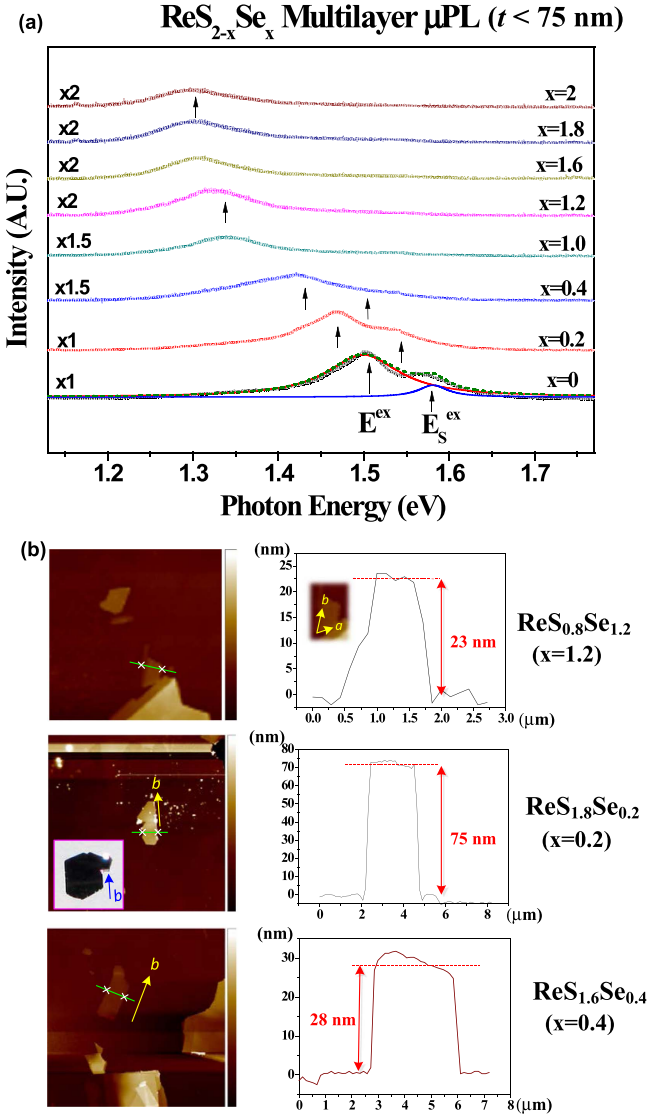

Figure 1. (a) The unpolarized μPL spectra of MLs in the series $ReS_{2-x}Se_x$ ($0 \leqslant x \leqslant 2$) with thickness less than 75 nm. The energies of the E^{ex} and E_S^{ex} peaks can be obtained from lineshape fits. (b) The AFM results of selected samples of $ReS_{0.8}Se_{1.2}$ ($t = 23$ nm), $ReS_{1.8}Se_{0.2}$ ($t = 75$ nm) and $ReS_{1.6}Se_{0.4}$ ($t = 28$ nm). The AFM images of the $ReS_{2-x}Se_x$ MLs essentially show a longer crystal edge along the b axis, which is easy to separate under mechanical stress as shown in the crystal inset.

the middle inset of the AFM image of $ReS_{1.8}Se_{0.2}$), the b axis (with Re_4 metal cluster chains) is easy to separate into a longer crystal edge under stress as shown in figure 1(b). Polarization-dependent μPL measurements with $E \parallel b$ and $E \perp b$ polarizations hence make it easy to identify the axial direction of the $ReS_{2-x}Se_x$ series MLs. All the $ReS_{2-x}Se_x$ series MLs in figure 1(a) are less than 75 nm thick. As shown in figure 1(b), the thicknesses of the $ReS_{0.8}Se_{1.2}$, $ReS_{1.8}Se_{0.2}$ and $ReS_{1.6}Se_{0.4}$ MLs are respectively 23, 75 and 28 nm. The unpolarized μPL spectra of the $ReS_{2-x}Se_x$ series shown in figure 1(a) reveal approximately two emission peaks denoted as E^{ex} and E_S^{ex} near the band edge. The energy positions of the E^{ex} and E_S^{ex} emissions are ~1.5 eV and ~1.57 eV in ReS_2, as obtained by Lorentzian lineshape fits. As the Se composition

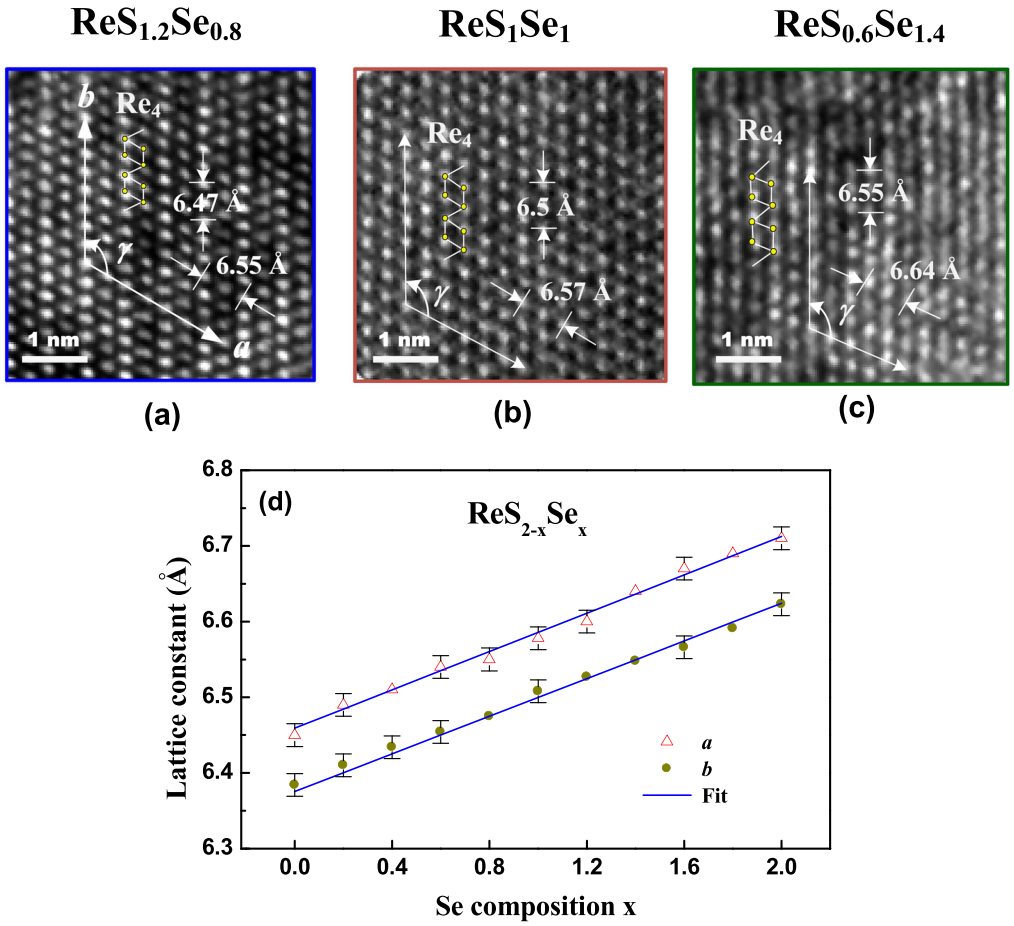

Figure 2. HRTEM images of three selected samples of (a) $ReS_{1.2}Se_{0.8}$, (b) ReS_1Se_1 and (c) $ReS_{0.6}Se_{1.4}$ multilayers. The Re_4 diamond-shape cluster chain and the orientations of *a* and *b* axes are also indicated. (d) The estimated in-plane lattice constants of *a* and *b* axes of MLs in the $ReS_{2-x}Se_x$ ($0 \leqslant x \leqslant 2$) series. The solid lines are fits using a linear relationship of Vegard's law.

of the $ReS_{2-x}Se_x$ is increased, the E^{ex} and $E_S{}^{ex}$ features show a reduction in energy and a broadening of the lineshape. The energy redshift (reduction) behavior of band edge excitons is similar to that shown by other TMDCs such as $MoS_{2-x}Se_x$ [26]. The slow decrease in energy as Se is substituted for S in $ReS_{2-x}Se_x$ indicates that the crystal structure and band structure of the entire series of $ReS_{2-x}Se_x$ ($0 \leqslant x \leqslant 2$) are similar.

To verify the constituent change and stoichiometric variation of the $ReS_{2-x}Se_x$ series, high-resolution transmission electron microscopy (HRTEM) is combined with energy-dispersive x-ray (EDX) measurements for the MLs. The stoichiometric content of $ReS_{2-x}Se_x$ with $x = 0$, 0.2, 0.4, 0.6, 0.8, 1.0, 1.2, 1.4, 1.6, 1.8 and 2.0 analyzed by EDX is approximately in agreement with the nominal starting composition within standard deviations (see SI). For simplicity, the value of x henceforth is defined by the starting composition. Figures 2(a)–(c) show the HRTEM images of three selected ML samples of $ReS_{1.2}Se_{0.8}$, ReS_1Se_1 and $ReS_{0.6}Se_{1.4}$ with an axis of the electron beam zone along [001] (i.e. the *c* axis). All the ternary $ReS_{2-x}Se_x$ samples in figure 2 clearly show the Re_4 diamond-shape clustering chains along the *b* axis in the layer plane, which are similar to that observed in binary ReS_2 and $ReSe_2$ [6]. As shown in figures 2(a)–(c), the marked regions and connections depict the Re_4 clustering chain in each of $ReS_{1.2}Se_{0.8}$, ReS_1Se_1 and $ReS_{0.6}Se_{1.4}$. The area of the Re_4 diamond shape in each sample increases as the Se content is increased. This result shows lattice dilation in the unit cell with the Se atom substituted for S. The lattice constants (calculated from atoms in the HRTEM images) are determined to be $a = 6.55$ Å and $b = 6.47$ Å for $ReS_{1.2}Se_{0.8}$, $a = 6.57$ Å and $b = 6.5$ Å for ReS_1Se_1, and $a = 6.64$ Å and $b = 6.55$ Å for $ReS_{0.6}Se_{1.4}$. Figure 2(d) depicts the measured lattice constants *a* and *b* of $ReS_{2-x}Se_x$ ($0 \leqslant x \leqslant 2$) with representative error bars from HRTEM estimation. The solid lines are fits of the measured lattice constants to a Vegard-like function with linear interpolation between the end members ReS_2 and $ReSe_2$. The fitting results obtained for the $ReS_{2-x}Se_x$ ($0 \leqslant x \leqslant 2$) MLs are $a(x) = (6.46 \pm 0.01) + (0.128 \pm 0.005)x$ Å and $b(x) = (6.38 \pm 0.01) + (0.126 \pm 0.005)x$ Å. In principle, the lattice constants varied linearly as Se substituted for S in $ReS_{2-x}Se_x$.

To characterize the property of dichroic emission in MLs of the $ReS_{2-x}Se_x$ series, polarized μPL measurements with light polarized linearly along and perpendicular to the *b* axis are respectively carried out on the *c* plane. The polarized μPL spectra of selected ML samples of ReS_2, $ReS_{1.8}Se_{0.2}$, $ReS_{1.6}Se_{0.4}$, $ReS_{0.8}Se_{1.2}$, $ReS_{0.4}Se_{1.6}$ and $ReSe_2$ using $E \perp b$ and $E \parallel b$ polarizations are shown in figures 3(a)–(f). The

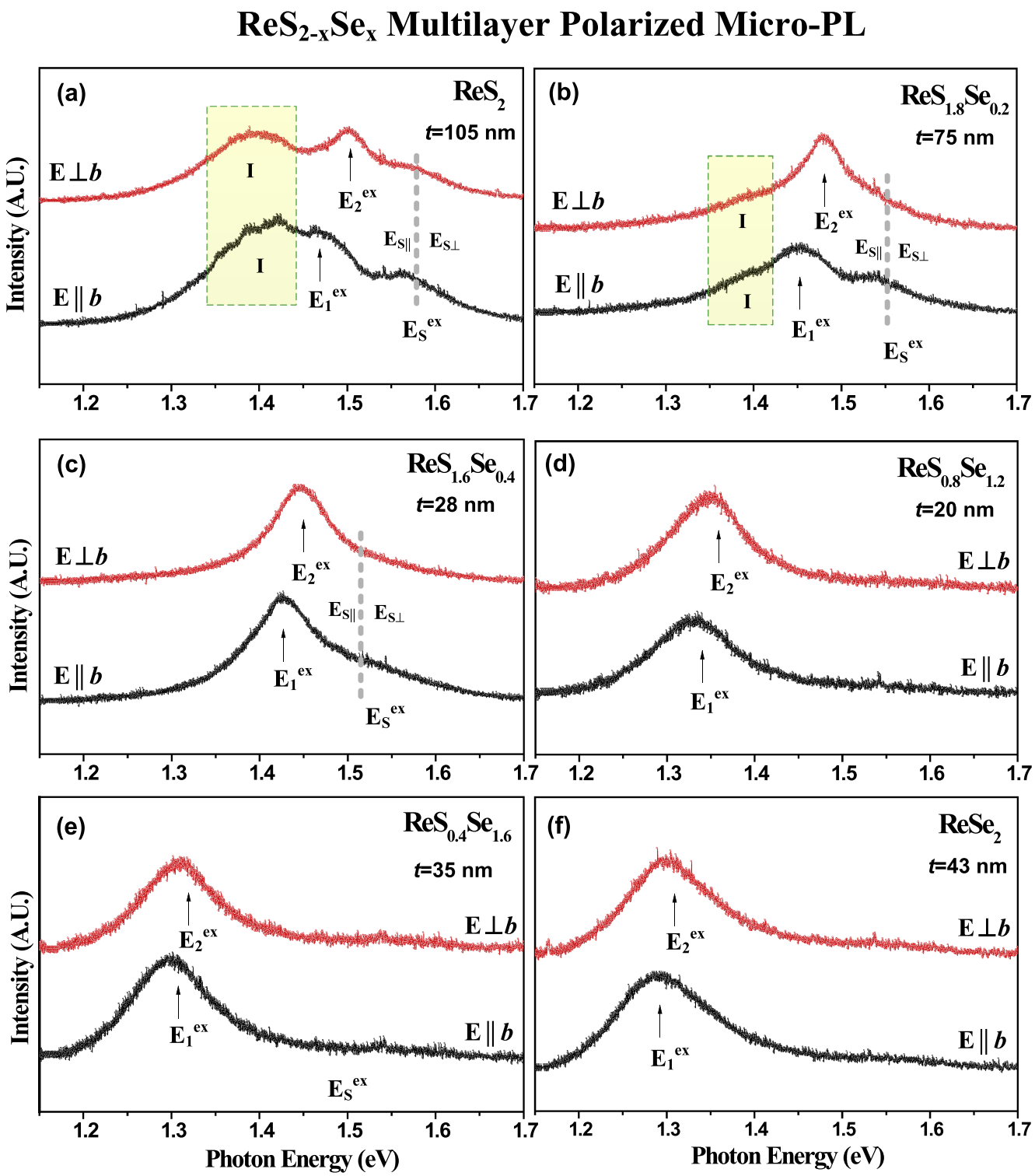

Figure 3. The polarized μPL spectra of selected $ReS_{2-x}Se_x$ ML samples of (a) ReS_2, (b) $ReS_{1.8}Se_{0.2}$, (c) $ReS_{1.6}Se_{0.4}$, (d) $ReS_{0.8}Se_{1.2}$, (e) $ReS_{0.4}Se_{1.6}$ and (f) $ReSe_2$ along the b axis and perpendicular to it. The thickness of each sample is also indicated.

thickness of the MLs and the identification of the b axis in $ReS_{2-x}Se_x$ were determined using AFM images such as those shown in figure 1(b). The ReS_2 MLs are about 105 nm thick. The polarized μPL spectra in figure 3(a) clearly show that the E^{ex} emission in figure 1(a) can be decomposed into E_1^{ex} ($\sim$1.463 eV, along $E \parallel b$) and E_2^{ex} ($\sim$1.502 eV, along $E \perp b$). They show clearly a polarization dependence similar to previous results from modulation spectroscopy (absorption) of excitonic transitions, $E_1^{ex} = 1.483$ eV and $E_2^{ex} = 1.522$ eV [8, 15]. The energy difference between polarized modulation spectroscopy and polarized μPL is about 0.02 eV. The energy of PL being slightly lower than that of modulation spectroscopy (absorption) is a general characteristic of semiconductors because excited hot carriers need some energy

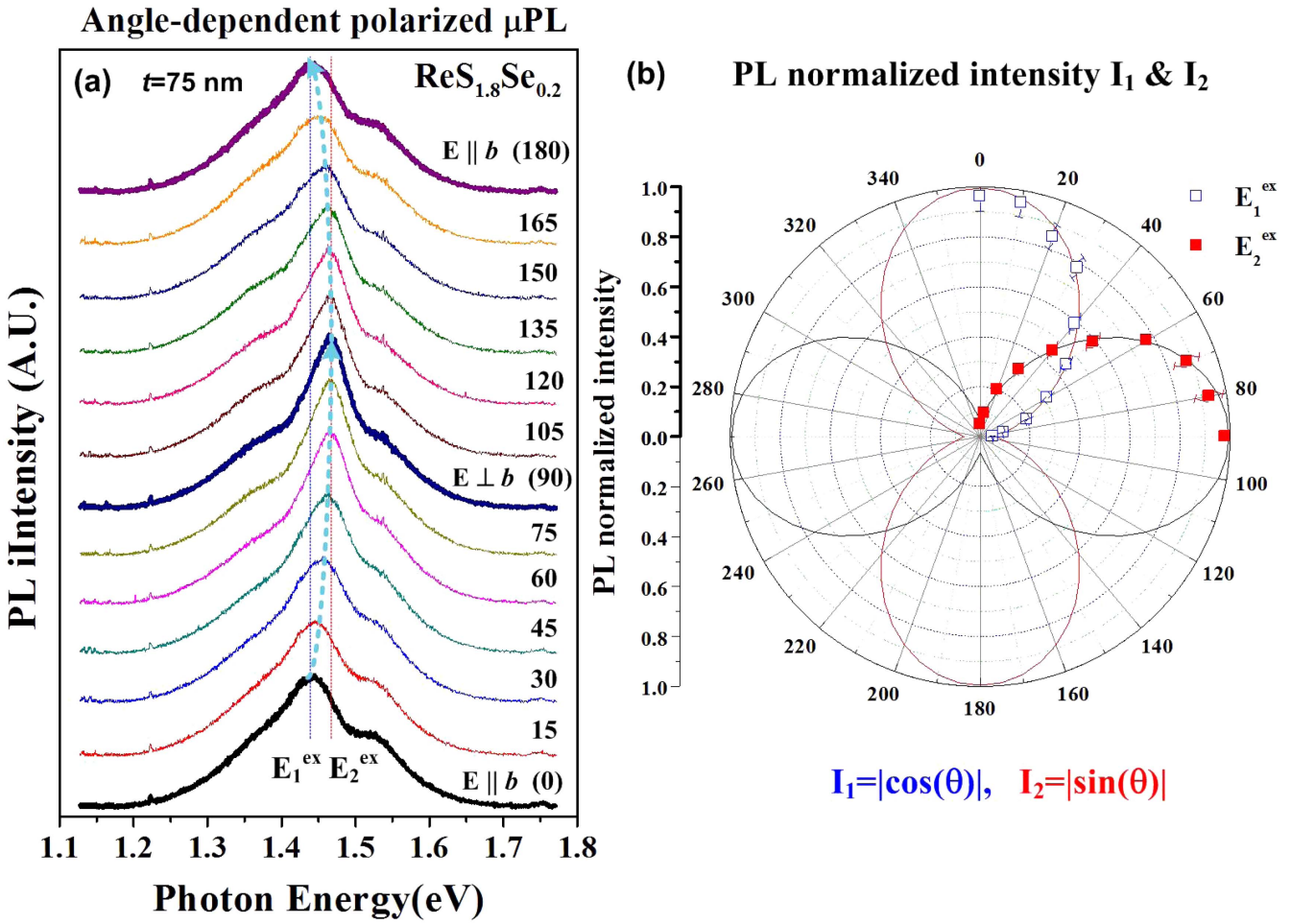

Figure 4. (a) Angular dependence of polarized μPL spectra of $ReS_{1.8}Se_{0.2}$ from 0° (via 90°) to 180°. (b) Polar plot of the normalized change in PL intensity of the E_1^{ex} and E_2^{ex} emissions.

relaxation before they recombine to emit light. As shown in figures 3(a)–(f), as the Se content increases in $ReS_{2-x}Se_x$, the energy positions of E_1^{ex} and E_2^{ex} decrease and the energy separations $\Delta E = E_2^{ex} - E_1^{ex}$ are reduced. The composition-dependent decrease in energy is similar to the result of thermoreflectance (TR) spectra of bulk $ReS_{2-x}Se_x$ ($0 \leqslant x \leqslant 2$) as shown in figure S2 in SI. To see the polarization dependence of the E_1^{ex} and E_2^{ex} features, angular-dependent μPL measurements of the MLs are carried out. Figure 4(a) shows the angular-dependent polarized μPL spectra of a selected sample of $ReS_{1.8}Se_{0.2}$ ($t = 75$ nm) with the linearly polarized light varying from 0° ($E \parallel b$) to 180° ($E \parallel b$) to show the dichroic emission behavior of E_1^{ex} and E_2^{ex}. The experimental results on two additional samples of ReS_2 and $ReS_{1.6}Se_{0.4}$ have also been included in figure S3 in SI for comparison. The normalized PL intensities of the two E_1^{ex} (I_1) and E_2^{ex} (I_2) emissions can be obtained from Lorentzian lineshape fitting and their polarization dependences are depicted in figure 4(b) for comparison. Essentially, $I_1 = |\cos(\theta)|$ for E_1^{ex} emission and $I_2 = |\sin(\theta)|$ for E_2^{ex} emission. At angles lying between $E \parallel b$ (0°, 180°) and $E \perp b$ (90°), the relative change in PL intensity of I_1 and I_2 renders the shift in energy position of the merged peak (E_1^{ex} and E_2^{ex}) sinusoidal as shown by the blue dashed line in figure 4(a). Also shown in figure 3, especially for the thicker MLs of ReS_2 ($t = 105$ nm) and $ReS_{1.8}Se_{0.2}$ ($t = 75$ nm), an additional emission feature denoted as I can be detected at ~1.4 eV for ReS_2 and at ~1.38 eV for $ReS_{1.8}Se_{0.2}$. The I feature may come from an indirect optical gap that had also been observed in the PL spectrum of bulk ReS_2 [27]. Furthermore, an emission feature E_S^{ex} positioned at ~1.572 eV can be clearly detected in the ReS_2 sample in figure 3(a). Similarly to E_1^{ex} and E_2^{ex}, the E_S^{ex} might also be an excitonic emission with a different origin. The E_S^{ex} emission is an excitonic series with clear polarization dependence along $E \parallel b$ and $E \perp b$ polarizations (denoted as $E_{S\parallel}$ and $E_{S\perp}$ in figures 3(a)–(c)), which has been found in previous low-temperature modulation spectroscopy results by absorption [8, 14]. The E_S^{ex} emission can be detected in the ML samples with lower Se content—ReS_2, $ReS_{1.8}Se_{0.2}$ and $ReS_{1.6}Se_{0.4}$—using polarized μPL measurements at 300 K (see figure 5(b)).

Figure 5(a) shows composition-dependent energy variations of E_1^{ex}, E_2^{ex} and E_S^{ex} of the $ReS_{2-x}Se_x$ series MLs with representative standard errors. The obtained values of $E_{S\parallel}$ and $E_{S\perp}$ (E_S^{ex}) for ReS_2, $ReS_{1.8}Se_{0.2}$ and $ReS_{1.6}Se_{0.4}$ are derived from the PL spectral analysis of figure 5(b). Figure 5(b) displays the polarization dependence of E_S^{ex} with $E \parallel b$ and E

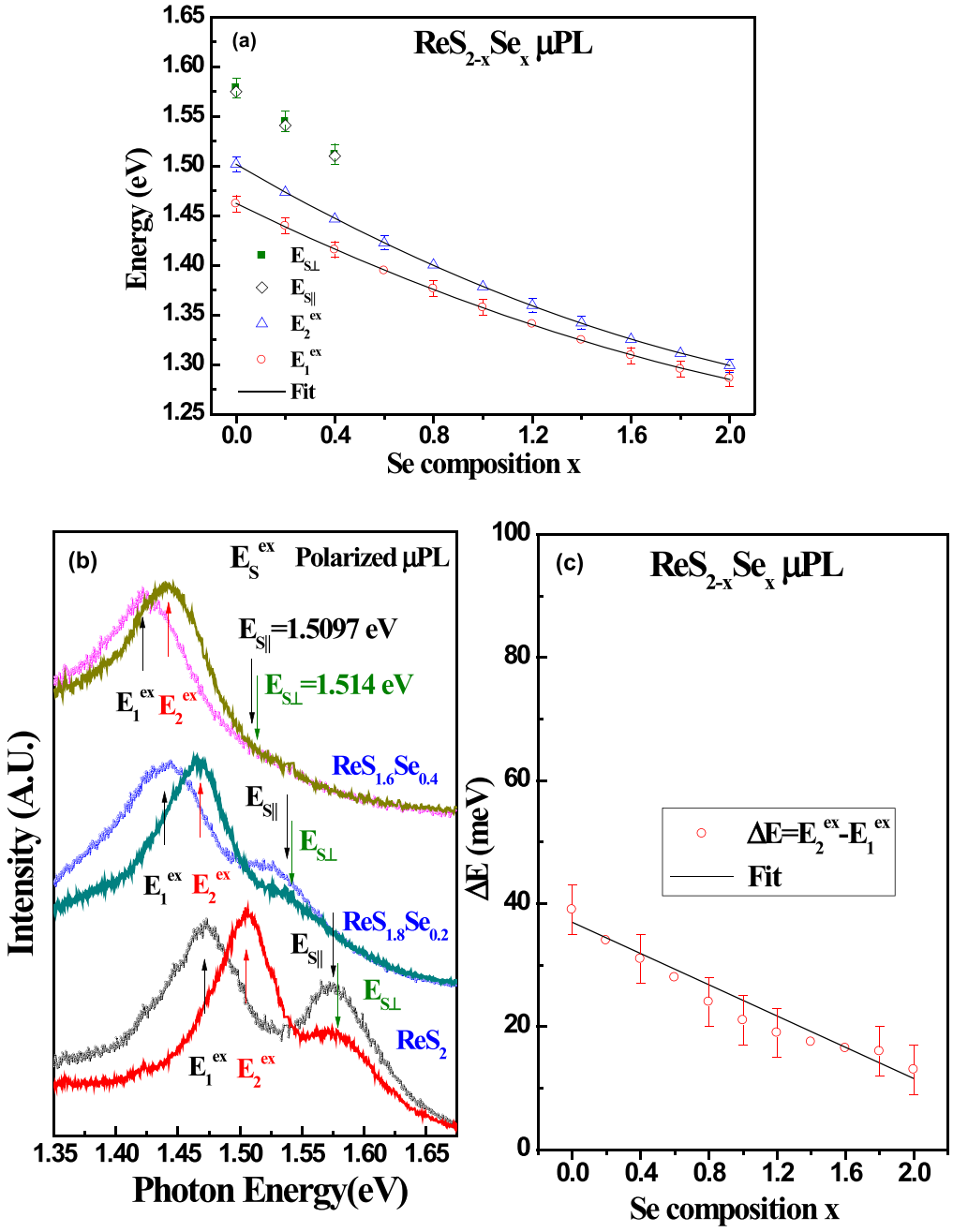

Figure 5. (a) Composition dependence of emission energies of E_1^{ex}, E_2^{ex} and E_S^{ex} detected in the $ReS_{2-x}Se_x$ ($0 \leqslant x \leqslant 2$) series MLs using polarized μPL measurements. (b) Polarized μPL spectra of $ReS_{1.6}Se_{0.4}$, $ReS_{1.8}Se_{0.2}$ and ReS_2. (c) The energy separation of $\Delta E = E_2^{ex} - E_1^{ex}$ as a function of Se content.

$\perp b$ polarizations for the three ML samples. The value of $E_{S||}$ is slightly lower than that of $E_{S\perp}$ ($\sim$4 meV) as shown in figure 5(b). The composition-dependent energy variation of E_1^{ex} and E_2^{ex} emissions can be analyzed with the formula $E(x) = E(0) + bx + cx^2$ for the series $ReS_{2-x}Se_x$ ($0 \leqslant x \leqslant 2$), where b is a linear change term and c is a bowing parameter [28]. The theoretical situation concerning band-gap bowing can be related to the nonlinear dependence of the crystal ion potential in the alloys. This results from the aperiodic variation of crystal potential in the substitution of S and Se in the mixed compound. The consequence should arise from the random variations in occupation sites of the chalcogen elements S and Se. The fitting results of composition-dependent energies are shown as solid curves in figure 5(a) and the obtained fitting parameters are $E(x) = (1.463 \pm 0.002) - (0.12 \pm 0.01)x + (0.017 \pm 0.002)x^2$ eV for E_1^{ex} and $E(x) = (1.502 \pm 0.002) - (0.14 \pm 0.01)x + (0.022 \pm 0.002)x^2$ eV for E_2^{ex}. The larger value of c for E_2^{ex} reveals that the valence-band splitting is more sensitive to the variation of crystal ion potential in the substitution of S and Se. Figure 5(c) shows the energy separation $\Delta E = E_2^{ex} - E_1^{ex}$ in the $ReS_{2-x}Se_x$ series. As the Se content is increased, the value

of ΔE decreases because the contribution of the Se ion potential tends to reduce the valence-band splitting in the crystal field environment. Figures 5(a) and (c) show that the composition-dependent energy variations of E_2^{ex} and E_1^{ex} contain bowing (i.e. the c factor) while the energy separation ΔE with Se content reveals only a linear dependence. The composition dependence of the band gap concerning bowing may correlate with the nonlinear dependence of the crystal ion potential in the $ReS_{2-x}Se_x$ series while the linear dependence of the energy separation ΔE may directly relate to the change in lattice constant. The composition-dependent change in ΔE in figure 5(c) is hence analyzed using the linear relation $\Delta E(x) = \Delta E(0) + mx$, where m is the slope. The fitting result is determined to be $\Delta E(x) = (37 \pm 3) - (12 \pm 2)x$ meV. Previous band-structure calculations [22, 23] show that E_1^{ex} and E_2^{ex} (with polarization dependence) may occur at the Γ point in the hexagonal Brillouin zone in the case of monolayer ReS_2 [22]. Because of the high asymmetry of the distorted 1 T layer, the general symmetric points of K–Γ–M of the normal MX_2 layer (e.g. MoS_2) will possess adjacent K′–Γ–M′ and next K″–Γ–M″ symmetric points in the monolayer ReS_2 [22]. The E_S^{ex} emission may originate from the critical-point transition of Γ–K2 (i.e. Γ–K″) of the distorted 1 T layer according to recent calculations [29]. The density-of-states (DOS) calculation in figure S4 also shows that the E_S^{ex} transition in ReS_2 comes from Re 5d t_{2g}–S 3p* ($3p_x^* + 3p_y^*$) antibonding states while E_1^{ex} and E_2^{ex} originate from Re 5d t_{2g}–Re 5d t_{2g}*. Further theoretical band-structure calculations and low-temperature μPL measurements need to be carried out to verify the origin of the transition of the E_S^{ex} exciton series. For the case of thick ReX_2, with many stacking monolayers, the minimum of the conduction band is still at the Γ point while the top of the valence band gradually flattens and shifts its upper maximum in the K′ direction [23], creating an indirect band gap. The indirect and direct emissions are hence simultaneously detected in the thicker ReS_2 and $ReS_{1.8}Se_{0.2}$ MLs (see figures 3(a) and (b)).

To further verify the indirect emissions (transitions) in the thick $ReS_{2-x}Se_x$ ($0 \leqslant x \leqslant 2$) MLs, μPL measurements are carried out on layers more than 1 μm thick. Figure 6(a) shows the unpolarized μPL spectra of the bulk $ReS_{2-x}Se_x$ ($0 \leqslant x \leqslant 2$) series. In comparison with the MLs with $t < 75$ nm in figure 1(a), the PL spectra of bulk $ReS_{2-x}Se_x$ show additional indirect emissions (e.g. denoted as I_1, I_2 and I_3 in ReS_2) together with the direct E^{ex} exciton emission (i.e. the combination of E_1^{ex} and E_2^{ex}) shown in figure 6(a). The coexistence of indirect and direct emissions can also be found in the other 2D compounds WSe_2 and MoS_2 that possess a stronger interlayer coupling effect [23], while they are only observed only in the very thin case (a few layers) [30] or with the auxiliary feature of hot-carrier injection to the indirect conduction-band valley by a Schottky contact junction [31]. For bulk MoS_2 and WSe_2 of greater thickness (i.e. indirect semiconductors), it is very hard to get direct-gap emission of PL. As shown in figure 6(a), for the bulk ReS_2, $ReS_{1.8}Se_{0.2}$, $ReS_{1.6}Se_{0.4}$, ReS_1Se_1 and $ReS_{0.8}Se_{1.2}$, the indirect resonant emissions (I_1–I_3) are clearly detected (with energies lower

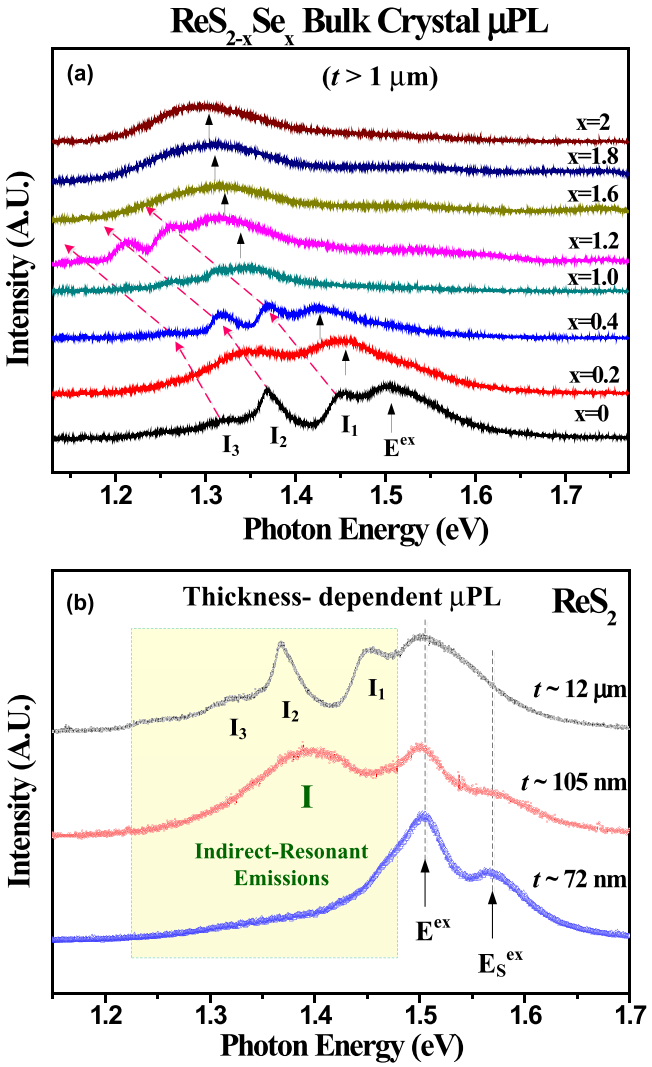

Figure 6. (a) The μPL spectra of bulk $ReS_{2-x}Se_x$ ($0 \leqslant x \leqslant 2$) crystals with the layer thickness greater than 1 μm. Strong indirect resonant emissions together with the direct E^{ex} emission are simultaneously detected. (b) Thickness-dependent μPL spectra of ReS_2 for the indication of direct and indirect emissions.

than that of direct E^{ex}), and they show a reduction in energy when the Se content is increased in $ReS_{2-x}Se_x$. In order to evaluate the effect of thickness on the enhancement of indirect resonant emission, thickness-dependent μPL measurements were also made. Figure 6(b) shows the thickness-dependent μPL spectra of ReS_2 with different thicknesses of 72 nm, 105 nm and 1200 nm. It is clear that the PL intensity and indirect resonant effect of the I feature (i.e. below the direct emission $E^{ex} \sim 1.5$ eV) decrease as the thickness is decreased. For $t < 72$ nm, the I feature is small and not detectable for the ReS_2 MLs as displayed in figure 6(b). A previous PL result showed that the direct PL peak (E^{ex}) of the monolayer ReS_2 will blueshift to ~1.6 eV [23]. However, the present μPL study confirms that the E^{ex} emission may sustain its PL intensity from MLs to the bulk, except that indirect resonant emission can be observed when $t > 70$ nm for the layered ReS_2. From this result,

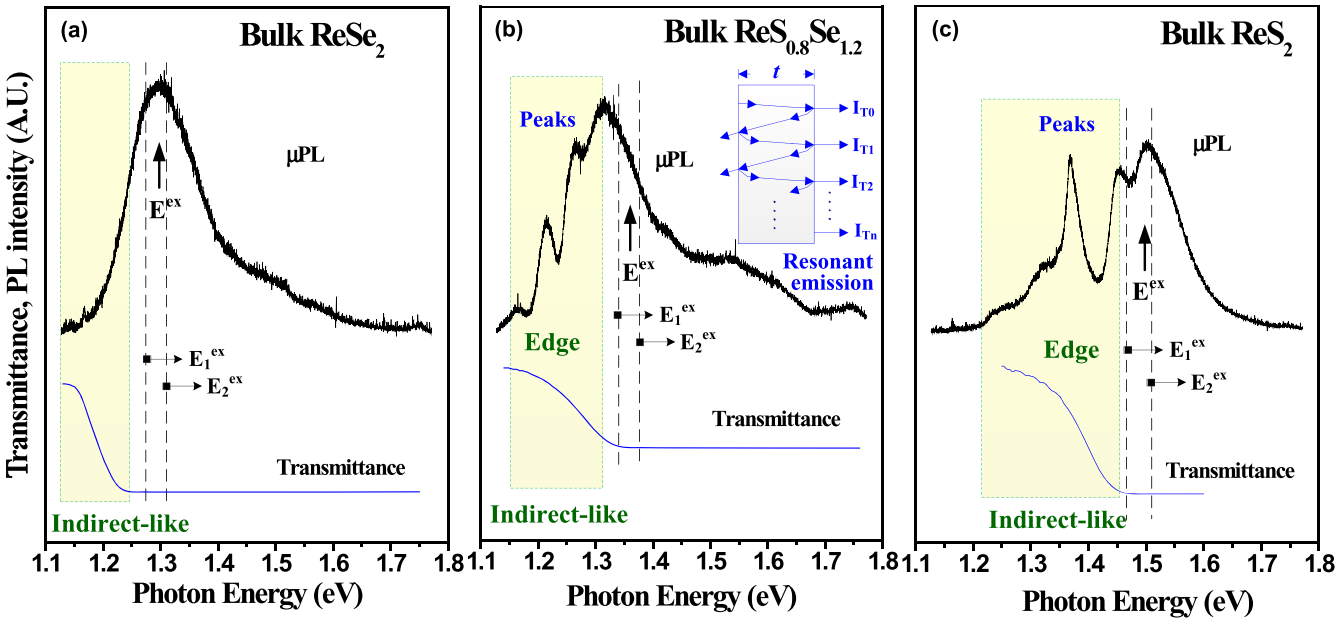

Figure 7. The comparison of μPL and transmittance spectra of three bulk samples of (a) $ReSe_2$, (b) $ReS_{0.8}Se_{1.2}$ and (c) ReS_2 to show their indirect and direct light emissions.

it is inferred that the relatively weaker coupling between monolayers via van der Waals potential interaction in ReX_2 (X = S, Se) might lead to the coexistence of direct and indirect resonant emissions in the bulk $ReS_{2-x}Se_x$. However, for the higher Se contents of $x = 1.6$, 1.8 and 2.0 in figure 6(a), the indirect resonant emission peaks are broadened and weakened because the exciton binding energies of E_1^{ex} and E_2^{ex} are lower than those of the other samples with lower Se contents of $x = 0$, 0.2 and 0.4 in the $ReS_{2-x}Se_x$ series. The broadened behavior of the excitonic transition features of the bulk $ReS_{2-x}Se_x$ can also be verified by the TR spectra shown in figure S2 in SI.

The transmittance was measured to verify the absorption edge of the bulk $ReS_{2-x}Se_x$. This is generally the direct way to check that the absorption edge is located at the direct gap. For a general direct-gap 2D semiconductor such as GeS [32] or GaSe [33], the location of the central energy of the transmittance absorption edge should match well with the direct emission peak in the bulk form. Figure 7 shows μPL and transmittance spectra of three representative bulk samples of $ReSe_2$, $ReS_{0.8}Se_{1.2}$ and ReS_2. It is clear that the transmittance absorption edge of each sample does not agree with the PL emission peak of E^{ex} (i.e. merged E_1^{ex} and E_2^{ex}), while the absorption edge matches well with the energy of the indirect resonant emission of each sample. The indirect absorption edge is at about 1.2 eV for $ReSe_2$, 1.25 eV for $ReS_{0.8}Se_{1.2}$ and 1.37 eV for ReS_2. The indirect resonant emission occurs by multiple internal reflections of a plate-type sample with a thickness t between two parallel interfaces (see the inset in figure 7(b)). Spectral interference fringes (peaks) can be generated when the emission is broadened (i.e. E^{ex}) and the Bragg condition is satisfied, i.e. $h\Delta\nu = hc/(2nt\cos\phi)$, where $h\Delta\nu$ is the energy spacing of two fringes, c the light speed, n the refractive index and $\cos\phi \approx 1$ if at nearly normal incidence.

Conclusion

In conclusion, the whole series $ReS_{2-x}Se_x$ ($0 \leqslant x \leqslant 2$) of layer crystals have been successfully grown by chemical vapor transport. The direct band-edge emissions of E_1^{ex} and E_2^{ex} show a clear polarization dependence of $E \parallel b$ and $E \perp b$ observed by μPL. This leads to two mutually orthogonal, linearly polarized beams of light being emitted from the $ReS_{2-x}Se_x$ MLs. When the Se content is increased, the energy separation $\Delta E = E_2^{ex} - E_1^{ex}$ decreases linearly. The variation in ΔE is similar to the change in lattice constant. For $t > 70$ nm, an additional indirect resonant emission feature I (which matches the energy portion of the indirect absorption edge) can be detected in the $ReS_{2-x}Se_x$ series below E_1^{ex}. The I features are enhanced and resonant when the layer thickness is greater than 1 μm (bulk). The direct and indirect light emissions can coexist in the bulk $ReS_{2-x}Se_x$ ($0 \leqslant x \leqslant 2$) layer crystals. The coexistence of direct and indirect emissions in bulk crystals of the $ReS_{2-x}Se_x$ series may be attributed to the in-plane anisotropy that arises from the Re_4 metal–metal bonding interaction to weaken the interlayer potential coupling between the ReX_2 monolayers. The $ReS_{2-x}Se_x$ layered materials are more suitable for application in polarized light-emitting devices in the NIR region from 1.2 to 1.6 eV.

Acknowledgments

We would like to acknowledge the financial support from the Ministry of Science and Technology, Taiwan under the grant No. MOST 104-2112-M-011-002-MY3. We are also more respectful to Professor Y S Huang (1949–2015) for all his contributions.

ORCID

Ching-Hwa Ho https://orcid.org/0000-0002-7195-208X

References

[1] Wilson J A and Yoffe A D 1969 The transition metal dichalcogenides—discussion and interpretation of the observed optical, electrical and structural properties *Adv. Phys.* **18** 193–335

[2] Wildervanck J C and Jellinek F 1971 The dichalcogenides of technetium and rhenium *J. Less-Common Met.* **24** 73–81

[3] Ho C H, Huang Y S, Liao P C and Tiong K K 1999 Crystal structure and band-edge transitions of $ReS_{2-x}Se_x$ layered compounds *J. Phys. Chem. Solids* **60** 1797–804

[4] Kelty S P, Ruppert A F, Chianelli R R, Ren J and Whangboo M-H 1994 Scanning probe microscopy study of layered dichalcogenide ReS_2 *J. Am. Chem. Soc.* **116** 7857–63

[5] Wang Q H, Kalantar-Zadeh K, Kis A, Coleman J N and Strano M S 2012 Electronics and optoelectronics of two-dimensional transition metal dichalcogenides *Nat. Nanotechnol.* **7** 699–712

[6] Lin Y C, Komsa H-P, Yeh C H, Björkman T, Liang Z Y, Ho C H, Huang Y S, Chiu P W, Krasheninnikov A V and Suenaga K 2015 Single-layer ReS_2: two-dimensional semiconductor with tunable in-plane anisotropy *ACS Nano* **11** 11249–57

[7] Whangbo M-H and Canadell E 1992 Analogies between the concepts of molecular chemistry and solid-state physics concerning structural instabilities. Electronic origin of the structural modulations in layered transition-metal dichalcogenides *J. Am. Chem. Soc.* **114** 9587–600

[8] Ho C H, Huang Y S, Tiong K K and Liao P C 1999 In-plane anisotropy of the optical and electrical properties of layered ReS_2 crystals *J. Phys.: Condens. Matter* **11** 5367–75

[9] Ho C H, Yen P C, Huang Y S and Tiong K K 2001 Polarized electrolyte-electroreflectance study of ReS_2 and $ReSe_2$ layered semiconductors *J. Phys.: Condens. Matter* **13** 8145–52

[10] Ho C H, Hsieh M H, Wu C C, Huang Y S and Tiong K K 2007 Dichroic optical and electrical properties of rhenium dichalcogenides layer compounds *J. Alloys Compounds* **442** 245–8

[11] Ho C H 2005 Optical study of the structural change in ReS_2 single crystals using polarized thermoreflectance spectroscopy *Opt. Express* **13** 8–19

[12] Tiong K K, Ho C H and Huang Y S 1999 The electrical transport properties of ReS_2 and $ReSe_2$ layered crystals *Solid State Commun.* **111** 635–40

[13] Ho C H 2013 Dichroic electro-optical behavior of rhenium sulfide layered crystal *Crystal Struct. Theor. Appl.* **2** 65–9

[14] Ho C H, Yen P C, Huang Y S and Tiong K K 2002 Photoreflectance study of the excitonic transitions of rhenium disulphide layer compounds *Phys. Rev.* B **66** 245207

[15] Ho C H, Lee H W and Wu C C 2004 Polarization sensitive behavior of the band-edge transitions in ReS_2 and $ReSe_2$ layered semiconductors *J. Phys.: Condens. Matter* **16** 5937–44

[16] Cui Q, He J, Bellus M Z, Mirzokarimov M, Hofmann T, Chiu H Y, Antonik M, He D, Wang Y and Zhao H 2015 Transient absorption measurements on anisotropic monolayer ReS_2 *Small* **11** 5565–71

[17] Liu E *et al* 2015 Integrated digital inverters based on two-dimensional anisotropic ReS_2 field-effect transistors *Nat. Commun.* **6** 6991

[18] Yang S *et al* 2015 Tuning the optical, magnetic, and electrical properties of $ReSe_2$ by nanoscale strain engineering *Nano Lett.* **15** 1660–6

[19] Corbet C M, McClellan C, Rai A, Sonde S S, Tutuc E and Banerjee S K 2015 Field effect transistors with current saturation and voltage gain in ultrathin ReS_2 *ACS Nano* **9** 363–70

[20] Zhang Q *et al* 2016 Extremely weak van der Waals coupling in vertical ReS_2 nanowalls for high-current-density lithium-ion batteries *Adv. Mater.* **28** 2616–23

[21] Gao J, Li L, Tan J, Sun H, Li B, Idrobo J C, Singh C V, Lu T M and Koratkar N 2016 Vertically oriented arrays of ReS_2 nanosheets for electrochemical energy storage and electrocatalysis *Nano Lett.* **16** 3780–7

[22] Ovchinnikov D, Gargiulo F, Allain A, Pasquier D J, Dumcenco D, Ho C H, Yazyev O V and Kis A 2016 Disorder engineering and conductivity dome in ReS_2 with electrolyte gating *Nat. Commun.* **7** 12391

[23] Tongay S *et al* 2014 Monolayer behavior in bulk ReS_2 due to electronic and vibrational decoupling *Nat. Commun.* **5** 3252

[24] Ho C H, Huang Y S, Tiong K K and Liao P C P C 1998 Absorption-edge anisotropy in ReS_2 and $ReSe_2$ layered semiconductors *Phys. Rev.* B **58** 16130–5

[25] Ho C H, Huang Y S and Tiong K K 2001 In-plane anisotropy of the optical and electrical properties of ReS_2 and $ReSe_2$ layered crystals *J. Alloys Compounds* **317–318** 222–6

[26] Wu Y J, Wu P H, Jadczak J, Huang Y S, Ho C H, Hsu H P and Tiong K K 2014 Piezoreflectance study of near band excitonic-transitions of mixed-layered crystal $Mo(S_xSe_{1-x})_2$ solid solutions *J. Appl. Phys.* **115** 223508

[27] Aslan O B, Chenet D A, van der Zande A M, Hone J C and Heinz T F 2016 Linear polarized excitons in single- and few-layer ReS_2 crystals *ACS Photonics* **3** 96–101

[28] Van Vechten J A and Bergstresser T K 1970 Electronic structures of semiconductor alloys *Phys. Rev.* B **1** 3351–7

[29] Zhong H-X, Gao S, Shi J-J and Yang L 2015 Quasiparticle band gaps, excitonic effects, and anisotropic optical properties of the monolayer distorted 1T diamond-chain structures ReS_2 and $ReSe_2$ *Phys. Rev.* B **92** 115438

[30] Zhao W, Ribeiro R M, Toh M, Carvalho A, Kloc C, Neto A H C and Eda G 2013 Origin of indirect optical transitions in few-layer MoS_2, WS_2, and WSe_2 *Nano Lett.* **13** 5627–34

[31] Li Z, Ezhilarasu G, Chatzakis I, Dhall R, Chen C C and Cronin S B 2015 Indirect band gap emission by hot electron injection in metal/MoS_2 and metal/WSe_2 heterojunctions *Nano Lett.* **15** 3977–82

[32] Ho C H and Li J X 2017 Polarized band-edge emission and dichroic optical behavior in thin multilayer GeS *Adv. Optical Mater.* **5** 1600814

[33] Wu C C, Ho C H, Shen W T, Cheng Z H, Huang Y S and Tiong K K 2004 Optical properties of $GaSe_{1-x}S_x$ series layered semiconductors grown by vertical Bridgman method *Mater. Chem. Phys.* **88** 313–7

Supplementary Information

Direct and indirect light emissions from the layered $ReS_{2-x}Se_x$ ($0 \leq x \leq 2$)

Ching-Hwa Ho[1,2,*], Zhan-Zhi Liu[1], and Min-Han Lin[1]

[1]*Graduate Institute of Applied Science and Technology, National Taiwan University of Science and Technology, Taipei 106, Taiwan*

[2]*Graduate Institute of Electro-Optical Engineering and Department of Electronic and Computer Engineering, National Taiwan University of Science and Technology, Taipei 106, Taiwan*

[*]E-mail: chho@mail.ntust.edu.tw

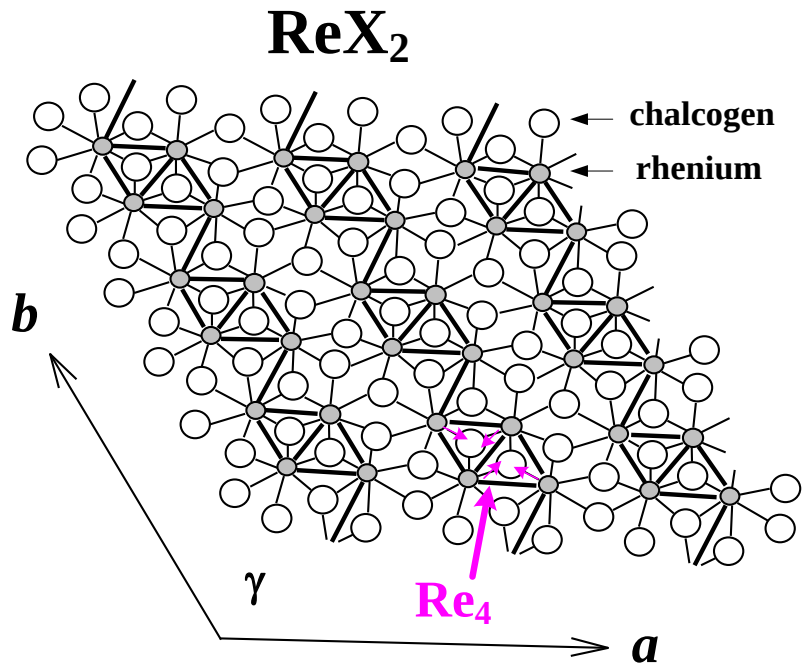

Figure S1. Atomic arrangement of ReX_2 (X=S, Se) in the layered plane. The hollow circles and gray circles are respectively the chalcogen and rhenium atoms. The 1-layer trigonal (1T) ReX_2 monolayer usually displays structural distortion owing to metal-metal bonding. The distortions of the ReX_2 lattice mainly come from the metal sheet with Re atoms comprising the Re_4 "diamonds" in the ReX_2 monolayers. As shown in the diamond-shape feature, the Re atoms will slip off from their regular octahedral sites forming many Re_4 units and which may couple each other to form one-dimensional clustering pattern of "diamond chains" along *b* axis in the Re metal sheet. The in-plane structural, mechanical, and optical anisotropy of ReX_2 will occur related to the orientation of the Re_4 clustering chain of *b* axis.

==========

Method

Crystal growth. Layered single crystals of $ReS_{2-x}Se_x$ ($0 \leq x \leq 2$) with various Se compositions of x=0, 0.2, 0.4, 0.6, 0.8, 1.0, 1.2, 1.4, 1.6, 1.8 and 2.0 were grown by chemical vapor transport (CVT) method [34, 35] using I_2 as a transport agent. The method consisted of two steps: First, prior to the crystal growth the powdered compounds of the starting material were prepared from the elements (Re: 99.99% pure, S: 99.999%, and Se: 99.999%) by reaction at 1000 °C for 10 days in evacuated quartz ampoules. To improve the stoichiometry, sulfur and selenium with 1 mol% in excess was added with respect to the stoichiometric mixture of the constituent elements. About 10 g of the elements were introduced into a quartz ampoule (22 mm OD, 17 mm ID, 20 cm length), which was then evacuated to a pressure of about 10^{-6} Torr and sealed. The mixture was slowly heated to 1000 °C. This slow heating is necessary to avoid any explosions due to the strongly exothermic reaction between the elements. For the single crystal growth, the chemical transport was achieved by an appropriate amount of material and transport agent (I_2 about 12 mg/cm^3) placed in a quartz tube (22mm OD, 17 mm ID, 20 cm length), which was then cooled with liquid nitrogen, evacuated to 10^{-6} Torr and sealed. The growth temperature was set as 1050 °C $\rightarrow$ 1000 °C with a gradient of -2.5°C/cm. The reaction kept 480 hrs for producing large single crystals. After the growth, synthetic $ReS_{2-x}Se_x$ ($0 \leq x \leq 2$) single crystals with maximum area size up to 1 cm^2 and thicknesses up to hundreds μm that formed silver colored and mirror-like crystalline surfaces were obtained. The weak van der Waals bonding between the layers means that the layered crystals can be separated from the *c* plane using razor blade or Scotch tape with mechanical exfoliation. The exfoliated multilayers with various thicknesses are then transferred to a SiO_2/Si substrate of dimension ~8×8×0.3 mm^3.

Optical characterization. The μPL measurements of the $ReS_{2-x}Se_x$ ($0 \leq x \leq 2$) series multilayers and bulk crystals were carried out by using a RAMaker integrated micro-Raman-PL identified system equipped with one 532-nm solid-state diode pumped laser as the excitation source. A light-guiding microscope (LGM) equipped with one Olympus objective lens (50x, working distance ~8 mm) acts as the inter-connection coupled medium between the layer sample, incident light, luminescence light, and the charge-coupled-device (CCD) spectrometer. A set of neutral density filters controlled the incident power of laser, and a dichroic sheet polarizer (operated in visible to infrared range) was utilized for the polarization-dependent measurements.

Measurement of transmittance at near-normal incidence was made on a scanning monochromatic measurement system with a resolution of 1Å. An 150 W tungsten-halogen lamp filtered by a PTI 0.2 m monochromator provided the monochromatic light. Transmission intensity was closely monitored to obtain an incidence as close to 90° as possible. Layer crystals with a thickness of about 1-15 μm were used for transmittance measurements.

For thermoreflectance (TR) measurement, the same monochromatic system as transmittance measurement was used. The TR experiments are carried out using indirect heating manner with a gold-evaporated quartz plate as the heating element [36]. The thin layered sample was closely attached on the heating element by silicone grease. The on-off heating disturbance uniformly modulates the ReX_2 (X=S, Se) layered samples periodically. An EG&G type HUV-2000B Si photodetector acted as the detection unit. The TR signal was measured and recorded via an EG&G model 7265 lock-in amplifier.

==========

$ReS_{2-x}Se_x$ ➔ The Results of Energy Dispersive X-ray Spectral Analysis

	x=0	x=0.2	x=0.4	x=0.6	x=0.8	x=1.0	x=1.2	x=1.4	x=1.6	x=1.8	x=2
Re (%)	33.15	33.01	33.81	32.78	34.42	32.23	34.28	32.28	32.89	33.25	33.61
S (%)	66.85	60.95	53.13	45.77	39.04	32.64	26.55	21.71	14.13	6.79	0
Se (%)	0	6.04	13.06	21.45	26.54	35.03	39.17	46.01	52.98	59.96	66.39

➔ For each of the $ReS_{2-x}Se_x$ sample, Re deviation < ±3 %, S deviation < ±5 %, and Se deviation < ±7 %

- EDX analysis of one selective sample:

$ReS_{0.6}Se_{1.4}$ EDX Mapping by TEM

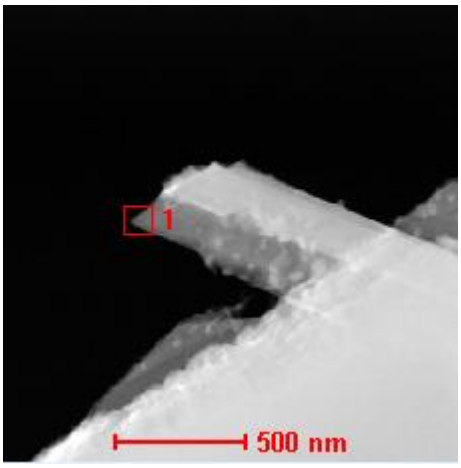

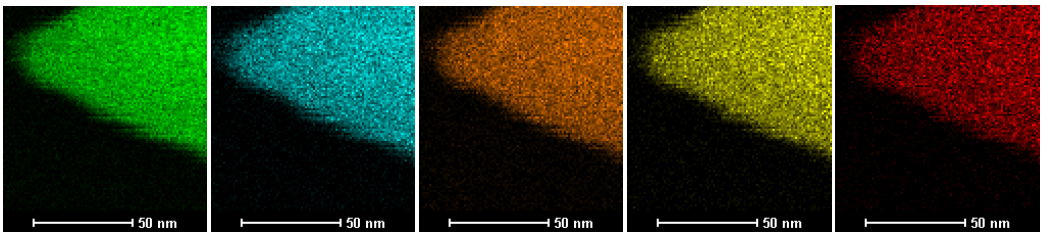

Re-L Re-m Se-K Se-L S-K

==========

Element	Weight (%)	Atomic (%)
Re (L)	58.13	32.28
S (K)	6.73	21.71
Se (K)	35.14	46.01

==========

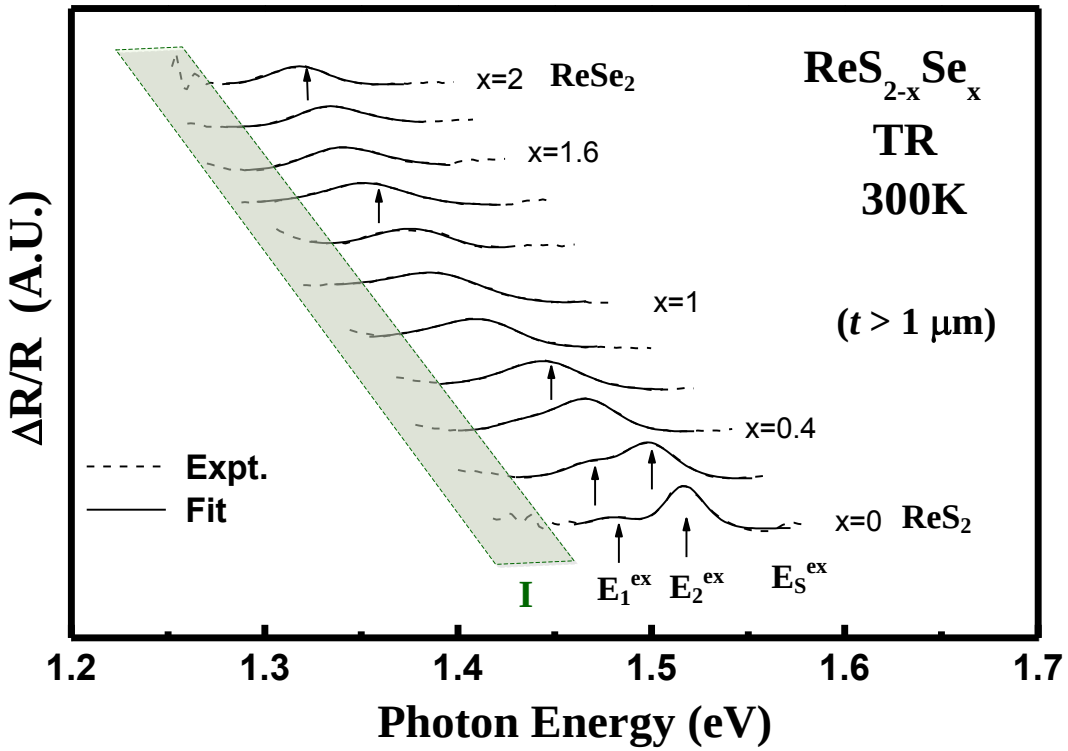

Figure S2. Experimental TR spectra of bulk $ReS_{2-x}Se_x$ ($0 \le x \le 2$) with a layer thickness larger than 1 μm. The dashed lines are the experimental data and solid lines are the least-square fits to a derivative Lorentzian line shape function appropriate for the excitonic-transition features for obtaining transition energies and broadening parameters [37]. The obtained transitions are indicated as E_1^{ex}, E_2^{ex} and E_S^{ex}, similar to those detected in the polarized μPL measurements in Figure 3. With the Se content is increased, E_1^{ex} and E_2^{ex} show energy reduction in the $ReS_{2-x}Se_x$ ($0 \le x \le 2$) series and a broadened I feature that corresponding to the indirect gap of the $ReS_{2-x}Se_x$ ($0 \le x \le 2$) was also detected below the direct E_1^{ex} transition. The I feature is correlated with the indirect resonant emissions of the μPL in the $ReS_{2-x}Se_x$ as those shown in Figure 6. With the Se content is increased, the E_1^{ex} and E_2^{ex} features are gradually broadened in the $ReS_{2-x}Se_x$ ($0 \le x \le 2$) series because the binding energy and energy separation of the E_1^{ex} and E_2^{ex} features are gradually decreased.

==========

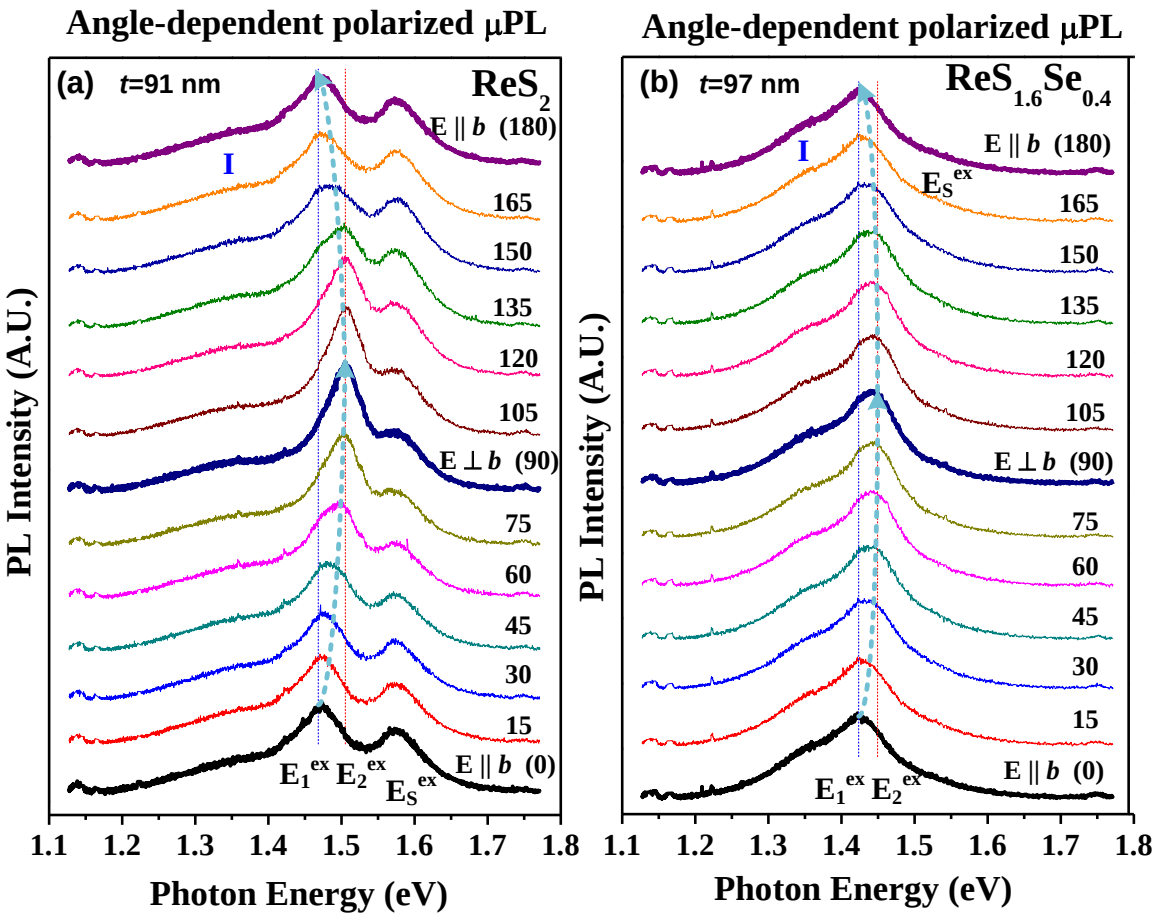

Figure S3. Angular-dependent polarized μPL spectra of (a) ReS_2 (t=91 nm) and (b) $ReS_{1.6}Se_{0.4}$ (t=97 nm) MLs with the polarization angles ranging from 0° to 180°. The results are implemented to demonstrate the dichroic behavior of normalized PL intensity change of the E_1^{ex} and E_2^{ex} emissions. The maximum intensity of E_1^{ex} emission is occurred at 0° and 180° (i.e. E || b polarization), while the maximum intensity of the E_2^{ex} emission is arisen at 90° (E ⊥ b polarization). As the linearly polarized angle varied from 0° to 90°, the normalized PL intensity change of E_1^{ex} and E_2^{ex} followed a sinusoidal variation trend of $I_1(\theta)=|\cos(\theta)|$ and $I_2(\theta)=|\sin(\theta)|$, such as those of $ReS_{1.8}Se_{0.2}$ shown in Figure 4(b). The indirect light emissions (I) of ReS_2 and $ReS_{1.6}Se_{0.4}$ are also detected owing to their thicknesses are larger than 70 nm.

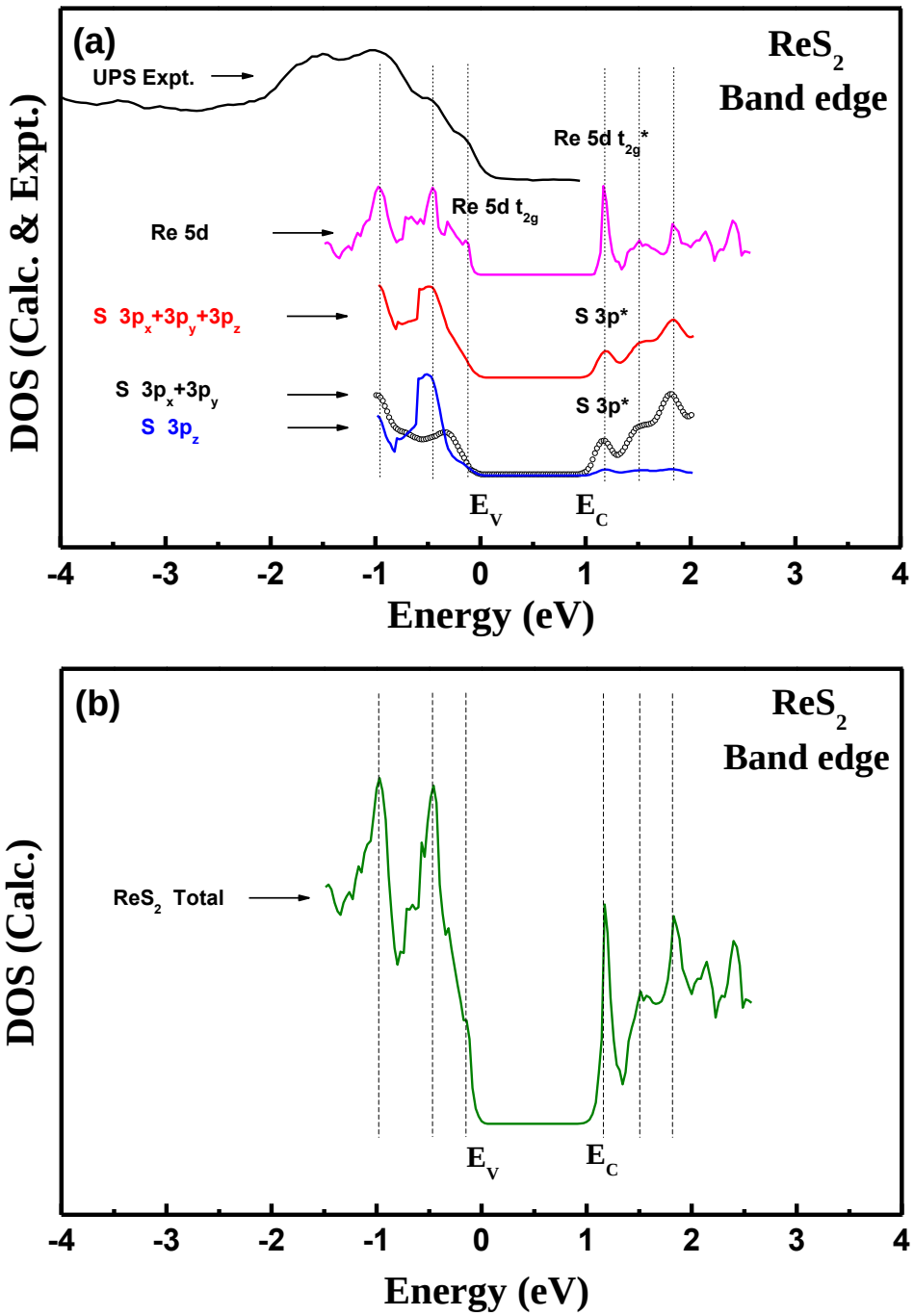

Figure S4. First principle density-of-states (DOS) calculations of the ReS_2 with distorted 1T layered structure of (a) partial DOS of Re 5*d*, S 3*p*, S $3p_x$+$3p_y$ and S $3p_z$, and (b) total DOS of ReS_2 near band edge. The experimental result of ultra-violet photo-electron spectroscopy (UPS) of the valence band is also included in (a) for comparison. The UPS results show the electron peaks match well with the DOS peaks of the valence band (E_V) in ReS_2. The partial DOS calculation indicates the E_V edge is composed of the Re 5*d* t_{2g} electrons while the conduction-band (E_C) edge mainly dominant by the mixed states of Re 5*d* t_{2g}^* and S 3*p** ($3p_x^*$+$3p_y^*$) antibonding states.

The E_1^{ex} and E_2^{ex} emissions in Figure 3 are assigned to come from the Re 5*d* t_{2g}^* to 5*d* t_{2g} recombination. The E_S^{ex} emission in Figure 5(b) is originated from S 3*p** ($3p_x^*+3p_y^*$) to the Re 5*d* t_{2g} transition. The E_1^{ex}, E_2^{ex}, and E_S^{ex} are originated from different origins in the ReX_2.

Supporting Information References:

[34] Sigiro, M.; Huang, Y. S.; Ho, C. H.; Lin, Y. C.; Suenaga, K. 2015 Influence of Rhenium on The Structure and Optical Properties of Molybdenum Disulfide. *Jpn. J. Appl. Phys.* **54**, 04DH05.

[35] Ho, C. H. 2011 Enhanced Photoelectric-Conversion Yield in Niobium-Incorporated In_2S_3 with Intermediate Band. *J. Mater. Chem.* **21**, 10518-10524.

[36] Ho, C. H.; Lee, H. W.; Cheng, Z. H. 2004 Practical Thermoreflectacne Design for Optical Characterization of Layer Semiconductors. *Rev. Sci. Instrum.* **75**, 1098-1102.

[37] Aspnes, D. E. in *Optical properties of solids*, *Handbook on Semiconductors, 2*, edited by M. Balkanski (North Holland, Amsterdam, 1980) p.109.